Noninvasive characterization of the Trecate (Italy) crude-oil contaminated site: links between contamination and geophysical signals

Giorgio Cassiani · Andrew Binley · Andreas Kemna · Markus Wehrer · Adrian Flores Orozco · Rita Deiana · Jacopo Boaga · Matteo Rossi · Peter Dietrich · Ulrike Werban · Ludwig Zschornack · Alberto Godio · Arash JafarGandomi · Gian Piero Deidda

Abstract The characterization of contaminated sites can benefit from the supplementation of direct investigations with a set of less invasive and more extensive measurements. A combination of geophysical methods and direct push techniques for contaminated land characterization has been proposed within the EU FP7 project ModelPROBE and the affiliated project SoilCAM. In this paper, we present results of the investigations conducted at the Trecate field site (NW Italy), which was affected in 1994 by crude oil contamination. The less invasive investigations include ground-penetrating radar (GPR), electrical resistivity tomography (ERT), and electromagnetic induction (EMI) surveys, together with direct push sampling and soil electrical conductivity (EC) logs. Many of the geophysical measurements were conducted in time-lapse mode in order to separate static and dynamic signals, the latter being linked to strong seasonal changes in water table elevations. The main challenge was to extract significant geophysical signals linked to contamination from the mix of geological and hydrological signals present at the site. The most significant aspects of this characterization are: (a) the geometrical link between the distribution of contamination and the site's heterogeneity, with particular regard to the presence of less permeable layers, as evidenced by the extensive surface geophysical measurements; and (b) the link between contamination and specific geophysical signals, particularly evident from cross-hole measurements. The extensive work conducted at the Trecate site shows how a combination of direct (e.g., chemical) and indirect (e.g., geophysical) investigations can lead to a comprehensive and solid understanding of a contaminated site's mechanisms.

Keywords Hydrogeophysics · GPR · ERT · Electrical methods · Cross-hole · Contamination

Responsible editor: Michael Matthies

G. Cassiani (✉) · J. Boaga · M. Rossi
Dipartimento di Geoscienze, Università di Padova, Padova, Italy
e-mail: giorgio.cassiani@unipd.it

A. Binley · A. JafarGandomi
Lancaster Environment Centre, Lancaster University, Lancaster, UK

A. Kemna · A. F. Orozco
Department of Geodynamics and Geophysics, University of Bonn, Bonn, Germany

M. Wehrer
Institut für Geowissenschaften, Friedrich-Schiller-Universität, Jena, Germany

A. F. Orozco
Department of Geodesy and Geoinformation, Technical University of Wien, Vienna, Austria

R. Deiana
Dipartimento dei Beni Culturali: Archeologia, Storia dell'Arte, del Cinema e della Musica, Università di Padova, Padova, Italy

P. Dietrich · U. Werban · L. Zschornack
UFZ-Helmholtz Centre for Environmental Research, Leipzig, Germany

A. Godio
Dipartimento di Ingegneria dell'Ambiente, del Territorio e delle Infrastrutture, Politecnico di Torino, Torino, Italy

G. P. Deidda
Dipartimento di Ingegneria Civile, Ambientale e Architettura, Università di Cagliari, Cagliari, Italy

Introduction

Conventional techniques for contaminated site characterization are based on drilling, sampling, and chemical analyses. Even though necessary and informative, these techniques are time-consuming, cost-intensive, and often do not adequately support decision making as they cannot cover the contaminated site in its full spatial extent. New techniques are therefore necessary. In particular, these techniques shall allow a stepwise site characterization strategy with possible feedbacks and adjustments. Among such techniques, a prominent role can be played by a range of near-surface geophysical techniques. Ground-penetrating radar (GPR, e.g., Annan 2005), electrical resistivity tomography (ERT, e.g., Binley and Kemna 2005), electromagnetic induction (EMI, e.g., Everett and Meju 2005), induced polarization and spectral induced polarization (IP/SIP, e.g., Binley and Kemna 2005), and self potential (SP, e.g., Revil et al. 2006) are among the techniques that lend themselves to these applications. All these techniques can focus with adequate resolution onto the first meters to tens of meters of subsoil, and possible links exist between the relevant measured physical quantities and the hydrological and environmental quantities of interest for contaminated site characterization (consider, e.g., Cassiani et al. 2006; Monego et al. 2010; Flores Orozco et al. 2011, 2012; Perri et al. 2012).

In general, geophysical techniques in environmental applications are used to characterize different aspects of the problem, namely, site structure, hydrology and hydrogeology, contamination, and bioattenuation.

Site structure

The identification of geological structure is a classical application of geophysical techniques, and contaminated site characterization is no exception. In addition, the mapping of anthropogenic structures (pipelines and foundations) at abandoned sites represents a standard application of geophysical methods (Everett and Meju 2005).

Hydrology and hydrogeology

The motion of fluids (air and water) can carry contaminants and put them in contact with potential receptors. One of the most elusive pathways is related to subsurface water migration; thus, the hydrological characterization of the site is extremely important. A vast number of hydrogeophysical studies have been devoted to the identification of flow and transport in the near subsurface, both in the vadose zone (e.g., Deiana et al. 2008) and in the saturated zone (e.g., Kemna et al. 2002). The advantage of this type of monitoring is fully established, and a wider application of these techniques to contaminated site characterization is expected.

Contamination

The localization and characterization of the spatial extent of contaminant distribution in the soil and subsoil are potentially significant results that geophysics could provide. However, direct detection of contaminants by means of geophysical methods has, so far, proved very problematic. This happens because even high contamination levels result in modest volume fractions which, in most cases, translate into weak signals for traditional geophysical methods (seismics, DC geoelectrics, gravity, magnetic, and electromagnetic methods). At a more attentive analysis, it is apparent that the problem lies not specifically in the low signal intensity that is often above the instrument sensitivity, but rather in the simultaneous presence of multiple signal sources, in addition to contamination, often having larger intensity and independent spatial and temporal distributions. These additional signal sources are mainly the (a) geological structure that is (for our purposes) time-invariant, and (b) the ambient dynamics, which is composed of a number of time-dependent phenomena, mostly of a hydrological nature (see above and, e.g., discussion in Binley et al. 2011). As contaminants often produce a weak signal, this is often overwhelmed by the other static and dynamic signals and often hardly recognizable. Misidentification of the contaminant target with other signal sources is very easy in such a framework and can hinder all efforts to use geophysics in contaminated site characterization. If the focus of characterization is on the identification of the contaminant location (the hazard, in the risk assessment procedure), then it becomes essential that the other signal sources (structure and hydrological dynamics) be fully understood in order to extract the residual signal coming from contamination. However, the process of contaminant detection is also helped, for certain categories of contaminants, by another important phenomenon: the associated biological activity. The biological activity often produces large physical signals, such as a marked increase in electrical conductivity (EC), that can help identify the areas where contaminant is used as a substrate by bacteria.

Bioattenuation

While contaminants themselves may be a weak source of geophysical signals, the biological activity associated to degradation of petroleum hydrocarbons is known to generate by-products that produces large electrical signals (e.g., Atekwana and Atekwana 2010). In these cases, geophysics can play a major role. Note that geophysical techniques can also provide estimates of the effectiveness of enhanced bioattenuation or other engineered remediation techniques (such as bioventing, air sparging, steam injection, etc.; e.g., Daily et al. 1995; Flores Orozco et al. 2011; Chen et al. 2012).

Within the framework of contaminated site characterization that essentially revolves around the idea of risk assessment (Petts et al. 1997), the first two aspects (structure and dynamics) concur at defining the possible pathways that can put contamination in contact with possible receptors, while the third and forth aspects (contamination and bioattenuation) are functional to the definition of hazard.

When considering in particular the case of contamination from hydrocarbon (light nonaqueous phase liquids or LNAPLs), biological processes play a fundamental role not only in the natural degradation of these contaminants but also, as a consequence of the produced by-products, in the possibility of detecting them via minimally invasive methods, particularly as a consequence of the increased EC of the system (Atekwana and Atekwana 2010). Numerous examples of the application of geophysical techniques to the detection and monitoring of hydrocarbon contamination have appeared in the literature over the past two decades (e.g., Benson et al. 1997; Bermejo et al. 1997; Sauck et al. 1998; Atekwana et al. 2000, 2002, 2004a; Osella et al. 2002; Werkema et al. 2003; Lopes de Castro and Branco 2003; Abdel Aal et al. 2006; Sogade et al. 2006; Bradford 2007; Cassidy 2007; Che-Alota et al. 2009; Gasperikova et al. 2012) and a comprehensive view of the state of the art is given by Atekwana and Atekwana (2010). The results of these geophysical studies have been somehow mixed. The application of the same geophysical technique at different sites and even at different locations on the same site can produce dramatically different results. This is largely dependent on the subsurface geology and hydrogeological conditions, i.e., on the structure of the individual site, that differ from site to site and produce geophysical signals larger, in general, than contamination itself. In addition, spatial and temporal characteristics of the contamination have an important bearing on the geophysical attributes and must be considered for proper interpretation. Note also that not all "aged LNAPL plumes" exhibit anomalous geophysical signatures associated with biodegradation (e.g., Tezkan et al. 2005). However, a few key facts have been ascertained and can be summarized as follows (see Atekwana and Atekwana 2010).

First, it has been long established that the presence of light hydrocarbons enhances the proliferation of microbes that use hydrocarbons as food. These microbes alter hydraulic properties as well as ionic composition of groundwater. Terminal electron acceptors (TEAs), such as oxygen, nitrate, manganese, iron, and sulfate, are necessary for the oxidation of hydrocarbons to the final by-products (CO_2 and water). The use of TEAs and production of CO_2 alters the redox state and can produce weathering of the solid matrix. During hydrocarbon biodegradation, the pore fluid chemistry is changed particularly by a decrease in the TEAs, the production of redox species, and the production of metabolic by-products such as organic acids, biosurfactants, and biogenic gases. The by-products of microbial action, such as organic and carbonic acid, can weather the solid matrix. These changes in pore fluid chemistry directly result in changes in electrolytic conductivity that can be measured, e.g., by DC resistivity methods.

Second, the strongest geophysical signals caused by contamination and biodegradation occur in the upper portion of the saturation zones and in the capillary fringe. In presence of an oscillating water table, very strong signals come from the smear zone where the residual hydrocarbon-free phase is in contact with the water moved by the fluctuations of the water table. The free-phase smearing also makes it more readily available for microbial activity (Lee et al. 2001). As this transition zone is also very rich in TEAs brought by the intense recharge dynamics, it is not surprising that this zone houses the most intense biodegradation and the highest populations of oil degrading microorganisms.

Third, the interpretation of the geophysical signals from hydrocarbon-contaminated sites must be accompanied by an understanding of the fine-scale variations in microbial processes, in particular, in the vertical direction (consider, e.g., Atekwana et al. 2005). Microbial processes vary over scales of tens of centimeters as a consequence of the partitioning of hydrocarbons into different phases and of the influx of TEAs (Atekwana et al. 2000, 2004a, b, c; Werkema et al. 2003).

It must be noted, however, that the subsurface contaminated by hydrocarbons is a dynamic and complex biophysicochemical environment (consider, e.g., the crude oil contamination at the Bemidji site; Baedecker et al. 1993; Bennett et al. 1993; Bekins et al. 2001), and its geophysical response will depend on a number of factors including the type of hydrocarbon and the release history. Therefore, the geophysical response of this type of contamination and associated biological processes is highly site-dependent.

In summary, the existing literature confirms that geophysical methods can be effectively used to study and monitor hydrocarbon contaminated sites. However, this is not a trivial task. The interpretation of geophysical data should be accompanied by a solid understanding of the microbial and geochemical context in order to avoid ambiguous conclusions.

In spite of these difficulties, geophysics can provide key information for contaminated sites in view of its capability of imaging the whole subsurface, potentially in a fully 3D manner and in its time evolution (e.g., Daily et al. 1992; LaBrecque et al. 1996). This high potential justifies the need for intensive basic research in this direction, particularly in view of the economical advantages of using less invasive investigation techniques. In order to address the above needs, the EU Framework Programme 7 (FP7) projects ModelPROBE, led by the Helmholtz Centre for Environmental Research (UFZ), Leipzig, Germany, and SoilCAM, led by the Norwegian Institute for Agricultural and Environmental Research (Bioforsk), Oslo, Norway, were funded and conducted from 2008 to 2012 (Kästner and

Cassiani 2009; French et al. 2009). The idea behind both ModelPROBE and SoilCAM was to integrate advanced geophysical site characterization techniques with new types of biological and chemical analyses as screening techniques. Based on these noninvasive surveys, the extent of sources, contamination levels, and soil heterogeneities must be characterized first. Hot spots shall then be investigated, e.g., by new, less invasive, direct push probing systems integrated with geophysical and hydrogeological methods, combined with chemical and isotopic contaminant analysis for source localization and identification.

The goal of this paper is to present the results of the investigations conducted at one of the study sites: the Trecate site (Northern Italy), with the following three specific aims:

(a) To assess the value of geophysical data for the definition of the site geological and hydrogeological structure.
(b) To define amplitude of dynamic geophysical signals, particularly caused by water table oscillations.
(c) To investigate to what extent, given our understanding of points (a) and (b) above, it is possible for geophysical techniques to help in contaminant localization, possibly with the support of local, direct ground-truthing.

Site description

The general, methodological aims of ModelPROBE and SoilCAM (see above) needed to be tested on well-characterized contaminated sites. One such site is located close to Trecate (Novara, Northwestern Italy). In 1994, the site was the scene of a crude oil spill following a blowout from an exploration well (named TR24, see Fig. 1). The incident resulted in approximately 15,000 m^3 of middle weight crude oil being released overland contaminating both soil and groundwater. The subsequent site remediation and resulting conditions have been reported elsewhere (e.g., Brandt et al. 2002). The site is characterized by a thick sequence of poorly sorted silty sands and gravels in extensive lenses, typical of braided river sediments. The Ticino river flows northwest to southeast a few kilometers east of the site. An artificial layer of clayey-silty material, about 1 m thick, placed as a liner for rice paddies about a century ago, overlies most of the site. The main zone of hydrocarbon contamination at the site covers approximately 96 hectares (Mage and Porta 2001). An anoxic, electrochemically reductive groundwater plume is present in the area, with limited extension to southeast from the site towards the Ticino River (Christensen et al. 2004). Both saturated and unsaturated zones are being monitored for natural attenuation and evolution of contamination conditions (Brandt et al. 2002). Significant levels of hydrocarbon

contamination remain also in the deep vadose zone as shown by the results of contamination measurements on the soil samples retrieved in recent years through direct push investigations to a maximum depth of 10 m (see Fig. 2; Brandt et al. 2002). Groundwater levels at the site show seasonal fluctuations of 5 to 6 m from about 6 to about 12 m below ground level, with higher levels experienced during the summer as a result of recharge from regional irrigation and flooding of the rice paddies (water table elevation is maximum at the end of September and minimum at the end of March; Cassiani et al. 2004).

The hydraulic properties of the local phreatic aquifer were determined in the past from pumping tests. The horizontal hydraulic conductivity and porosity have average values of 56 m/day and 29 %, respectively. The vertical hydraulic conductivity was estimated to be 3.4 m/day in the saturated zone using borehole dipole techniques (Burbery et al. 2004) and 0.61 to 1.46 m/day in the unsaturated zone by calibrating vadose models on time-lapse VRP data (Cassiani et al. 2004).

The characteristics of the Trecate site make it, in many respects, an excellent test site for the goals of the projects. In particular, at this site we do not find the usual abundance of man-made subterranean structures so common in the majority of contaminated sites. Such utilities can have a strong geophysical signal that can mask other, more subtle signals linked to contamination and biodegradation. However, other complexities exist at the Trecate site. For example, the site has large water table seasonal oscillations, making the separation of static and dynamic aspects of the geophysical signals challenging, and requires that repeated time-lapse data be acquired.

Geophysical monitoring at the trecate site

From May 2009 to September 2012, ERT, GPR, IP/SIP, SP and EMI measurements were conducted at the Trecate site with the aim of characterizing the structure and contamination distribution in the shallow subsurface. Here, we focus on the evidence derived from the combination of ERT, GPR, and EMI data, supported also by direct push EC logs. ERT and GPR measurements were conducted on a number of lines across the site. However, the most interesting results can be derived from the data collected along two reference profiles (see Fig. 2) that are located in the heavily contaminated region (line A–A′) and the uncontaminated region (line B–B′), respectively. Within the SoilCAM project, some monitoring boreholes were also drilled along these two lines, forming two pairs of neighboring holes (Fig. 2) indicated in the following as 2009 SoilCAM boreholes (in the contaminated zone) and 2011 SoilCAM boreholes (in the uncontaminated zone). The borehole pairs reach a depth of about 17 m in the contaminated zone and 14 m in the uncontaminated zone

Fig. 1 **a** A photo of the crude TR24 oil well blowout in Trecate, Novara, Italy in 28 February 1994. The *insets* show: **b** the location of the site in Italy and **c** a satellite image showing the extent of oil spread shortly after the accident
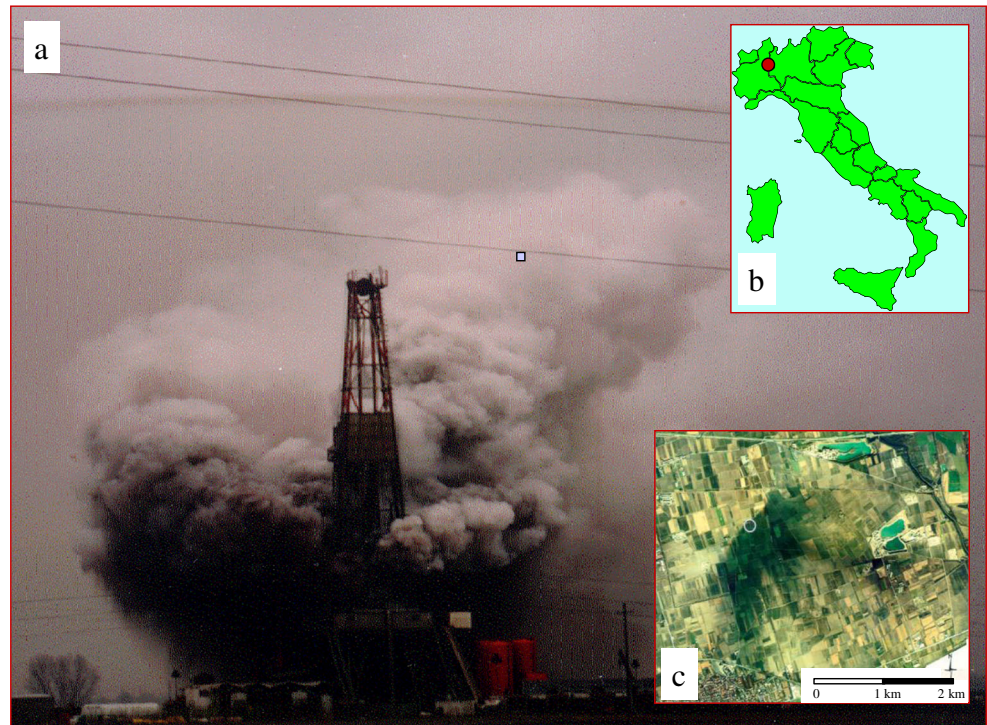

below ground, respectively. Each hole is equipped with 24 evenly spaced electrodes, thus allowing a cross-hole ERT acquisition with very good spatial resolution, in the meter range. The boreholes in each pair are spaced at a fraction of their depth, i.e., 6 m for the 2009 SoilCAM boreholes and 3.95 m for the 2011 SoilCAM boreholes, respectively.

Surface ERT acquisitions

Measurements were performed using an IRIS Syscal Pro resistivity meter, deploying 48 stainless-steel electrodes with a separation of 2.5 m. We used a "skip-3" (four-electrode dipole separation) dipole–dipole measurement protocol, which means the current and potential dipoles have a length of 10 m (skipping three electrodes between positive and negative poles in current and potential dipoles) and with a maximum separation between current and potential dipoles of 37 electrodes. This scheme provides a good signal-to-noise level (given the relatively large size of the dipoles) and is still a good spatial resolution. The total line length of B–B′ is 120 m, and we consider reliable the inverted results to a depth of at least 15 m. This is evaluated on the basis on the rule-of-thumb

Fig. 2 Map of the Trecate site showing the extent of the areas exceeding 500 mg/kg total petroleum hydrocarbon (*TPH*) in soil at two depths (4 and 10 m below ground) as derived from historical (since 1995) direct push sampling data, together with the two main investigation profiles selected for this study (*line A–A′* and *line B–B′*). The locations of the two pairs of boreholes drilled for cross-hole geophysical investigations are also shown
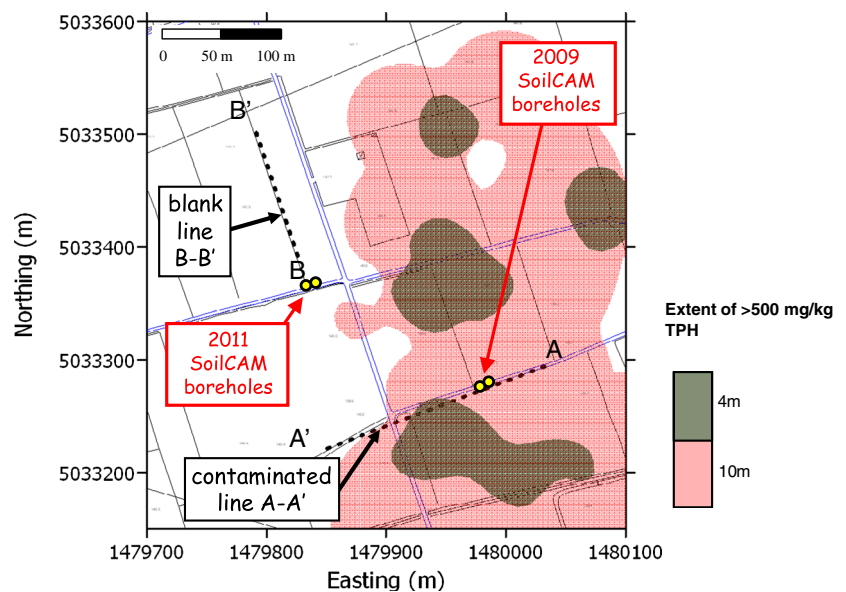
that wants the depth of penetration be a fraction (e.g., 1/5) of the total array length, considering also precautionally that dipole–dipole schemes tend to become less reliable with depth. Along line A–A′, we performed the measurements using 48 electrodes in roll-along (for a total of 81 electrodes) reaching a total length of 200 m, but still the depth of investigation is the same as for line B. All data (1,745 and 722 quadrupoles in arrays A and B, respectively) were measured in normal and reciprocal configurations to allow data error estimation based on normal-reciprocal discrepancies (e.g., Binley et al. 1995). Resistance data were collected in the time domain, using a square-wave current injection with 50 % duty cycle and a pulse length of 2 s. For the inversion of resistance data, the data error was estimated by a linear model. Outliers were defined as those associated with a difference between normal and reciprocal larger than two times the standard deviation from the normal/reciprocal misfit from the entire dataset (as described in Flores Orozco et al. 2012), resulting in a removal of approximately 10 to 15 % of the measurements. The error parameterization were implemented in a smoothness-constrained inversion algorithm implemented in R2 (www.es.lancs.ac.uk/people/amb/Freeware/R2/R2.htm and detailed in Binley and Kemna 2005), which was used to perform the inversion of the data here presented.

Surface GPR acquisitions

The surface GPR profiles were acquired using a Sensors & Software PulseEkko Pro system with 100 MHz antennas. The results presented here correspond to a minimum-offset acquisition, while GPR velocities were estimated from several common midpoint (CMP) surveys along each profile (for technical details, see, e.g., Annan 2005).

EMI mapping

Extensive frequency-domain electromagnetic mapping was conducted over all the accessible areas of the site, using a GF Instruments CMD-4 sonde, having a nominal depth of penetration of about 6 m. The goal was to give a large-scale picture of the shallow subsurface, also in search of possible man-made artefacts. For a description of the EMI techniques, consider, e.g., Everett and Meju (2005).

Cross-hole acquisitions

The availability of the SoilCAM boreholes made it possible to conduct cross-hole geophysical investigations both in the contaminated and the uncontaminated areas (see Fig. 2). Cross-hole investigations allow for a much better resolution (in the meter range) at depth and thus allow us to investigate in situ processes such as contaminant distribution and biodegradation in their spatial variability at a relatively fine scale.

Cross-hole ERT was run with the same equipment as for surface measurements. We used the same dipole–dipole skip-3 measuring protocol used in surface acquisitions for a total of 722 quadrupoles. Each measurement was also collected also as a normal reciprocal pair and outliers were also defined as those with a large normal reciprocal misfit. Again inversion was made using the R2 software.

Cross-hole GPR data were collected on the same borehole pairs using the PulseEkko Pro system with 100 MHz borehole antennas. Two acquisition schemes were used, i.e., (1) a multiple offset gather (MOG) with 0.5 m vertical spacing between antenna stations and (2) a zero offset profile (ZOP) with 0.25 m spacing between antenna stations. In both cases, the information is mainly contained in the GPR travel time associated to each transmitter–receiver pair, as this depends on the dielectric constant and thus, mainly, on the volumetric soil moisture content (Annan 2005). In the case of MOG, a tomographic inversion is needed, which can yield a 2-D distribution of electromagnetic velocity and consequently of electrical permittivity that depends strongly on soil moisture content (e.g., Deiana et al. 2008), while in the case of ZOP, generally at each depth, it is possible to obtain independently an estimate of average permittivity and moisture content (e.g., Rossi et al. 2012).

Direct push EC logs

The joint use of geophysical methods and direct push measurements and sampling is becoming state of the art for shallow investigations (e.g., Schütze et al. 2012) and is one of the approaches endorsed in the ModelPROBE project. At the Trecate site, direct push was used to retrieve soil samples and to provide detailed vertical EC logs at the selected locations. These logs allow for local verifications of the accuracy and resolution of the surface ERT lines.

Geochemical monitoring and contamination at the trecate site

A multilevel sampling system was installed at the Trecate field site in early December 2009. The tubing system is a CMT Multilevel system 503 (Solinst, Canada) with four piezometers housing seven sampling ports each (Fig. 3). Close spacing of the sampling ports (as close as 0.4 m) was chosen to support the interpretation of geophysical data. The boreholes BS5, BS6, BS7, and BS8 were constructed in distances of 1 m on the side of the dirt road roughly between the two 2009 SoilCAM boreholes, where regular ERT and GPR cross-borehole measurements are made (Fig. 3). Soil core samples were taken from the two boreholes BS5 and BS7. Three sampling campaigns were carried out: 30 August −04 September 2010; 11 October–15 October 2010, and 10 May–12 May 2011. Port purging and stabilization of physicochemical online measurements were achieved before each

Fig. 3 Multilevel sampler system installed between 2009 SoilCAM boreholes in the contaminated zone (see Fig. 2)
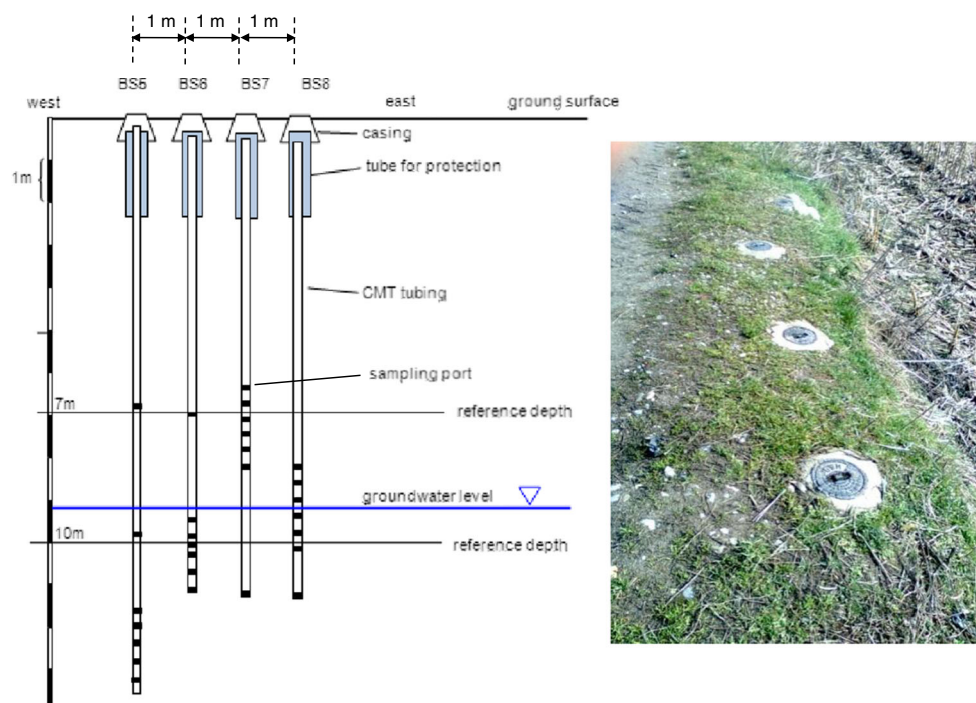
sampling. In addition to the multilevel piezometers, two wells (B-A and B-A2) outside the contamination zone were sampled to derive the background values.

Dissolved oxygen, EC, redox potential, pH, and CO_2 were analyzed online in flow through-cells with ion selective electrodes (WTW, Weilheim, Germany) during pumping on site. Nitrate (NO_3^-), nitrite (NO_2^-), ammonia (NH_3), sulfide (S^{2-}), iron (Fe^{2+}), manganese (Mn^{2+}), and turbidity were determined photometrically (Kolorimeter DR890, Hach Lange, Düsseldorf, Germany) on site immediately after sampling. Samples for laboratory analysis were kept refrigerated immediately after sampling. The samples for laboratory analyses were filtered in the field [except samples used for analyses of total organic carbon (TOC) and total petroleum hydrocarbons (TPH)] with a 0.45-μm filter with Supor® membrane, and samples for inductively coupled plasma optical emission spectrometry (ICP OES), samples for analyses of TOC, and dissolved organic carbon (DOC) were additionally acidified immediately after sampling. Sulfate (SO_4^{2-}), nitrate (NO_3^-), and chloride (Cl^-) were analyzed with ion chromatography. TOC and DOC were determined as nonpurgeable organic carbon with a total carbon (TC) analyzer (multi N/C 2100, Analytic Jena, Jena, Germany). Total inorganic carbon (TIC) was determined as purgeable carbon after acidification. Total calcium, magnesium, sodium, potassium, iron, and manganese were determined by ICP OES. For TPH, the aqueous samples were prepared and analyzed according to EN ISO 9377–2:2000. The sample of 200 ml was extracted with 10 ml of hexane during 30 min of intense stirring. The hexane phase was separated from the aqueous phase in a separatory funnel

and percolated through Florisil columns overlaid with 0.5 g Na_2SO_4. The column with the Na_2SO_4 was washed two times with 5 ml hexane. The hexane phase was reduced in volume to exact 1 ml using first a multivapor and then N_2 stream. This sample volume was transferred into a GC vial and measured with GC-FID. The 2 μl sample was injected splitless into a Trace GC Ultra (Thermo Scientific) with an injection temperature of 300 °C. The GC temperature program was as follows: 40 °C (1 min), 15 °C/min to 120 °C and 30 °C/min to 340 °C (10 min). The FID was set to 350 °C with air flow of 350 ml/min, H2 35 ml/min, and makeup gas 30 ml/min. Carrier gas helium was 1 ml/min, and the column was a Rxi-1HT with dimensions: 15 m, 0.25-mm ID, and 0.1-μm film.

Among other parameters, TC and TOC were determined in the core soil samples by oxidative combustion of 100 to 200 mg air-dried, homogenized sample material in a high-temperature furnace at 1,300 °C (multi N/C 2100, Analytic Jena). TOC was determined after fumigation of carbonates with HCl. TIC was calculated as the difference between TC and TOC. TPH extraction was carried out on two parallel samples of 5 g of the air-dried and homogenized sample. The sample was filled layerwise with 2 g quartz sand, 2 g Na_2SO_4 into 11 ml ASE cells, and extracted in two steps, one at room temperature and one at 100 °C (pressure=1,450 psi) with hexane. The extracts of the two steps were unified and cleaned up over 5 g Silica (9 % deactivated) and 5 g Alox (5 % deactivated). A retention time marker was added, and the sample was reduced to 5 ml with a rotary evaporator. An aliquot of 1 ml was transferred to the GC vial. The GC-FID analysis was carried out as described for the aqueous samples.

The presence of hydrocarbon contamination in the subsurface is apparent even from direct access to the 2009 SoiLCAM boreholes (see Fig. 4). However, what looks like oil-free phase is, in fact, for the most part a brown oil phase emulsion in aqueous phase (Fig. 4). The presence of such an emulsion is likely to occur as an effect of the pronounced water table oscillation, similar to the effect described in the model for the release of colloidal droplets from a NAPL phase under flow conditions (Pumphrey and Chrysikopoulos 2004). Also, the production of bioemulsifiers as a result of microbial activity can result in stable emulsions (Willumsen and Karlson 1997). Note that the biodegradation of hydrocarbons at the Trecate site is a well-established fact (e.g., Burbery et al. 2004).

Results and discussion

Surface ERT, GPR, EMI, and EC logs

The results of the surface ERT and GPR acquisitions clearly show some of the key features of the Trecate shallow subsoil. In particular, line B–B′ (in the uncontaminated zone) shows very regular features that are consistent with the relatively simple site's geology. No feature in this image appears to be consistent with absence of contamination (Fig. 5). The vadose zone, down to the water table at 6- to 12-m depth depending on the season, reaches resistivity values of over 2,000 Ohm m, perfectly compatible with an unsaturated gravel (Fig. 5). Below the water table, resistivity drops at most to a few hundred Ohm m. Note that the ERT results along this line are confirmed by the EC logs (see the EC vertical profiles shown in Fig. 5a). The only remaining feature in the

uncontaminated line B–B′ is a shallow low-resistivity channel to a depth of 2–2.5 m that is also perfectly visible as a reflector in the GPR profile (Fig. 5). Similar features are actually common across the site and correspond to the natural palaeo-channels created by a braided river (the ancient Ticino), now filled with fine (silty) sediments as testified also by their relatively low resistivity values.

Limited changes are observed between geophysical data collected at different time instants. More pronounced differences are observed between different locations. For example, Figs. 5 and 6 compare the contaminated and the uncontaminated reference profiles. Figure 6 shows the ERT and GPR results along line A–A′ that crosses the most heavily contaminated zone. The most notable characteristics of these results, particularly of the ERT image, is the much more heterogeneous picture that is given of the subsurface. Here too, like in line B–B′, there is a shallow low-resistivity palaeo-channel reaching a depth of 3 to 4 m, which is also visible as a reflector in the GPR profile, even though the higher EC of the filling material limits GPR penetration, so the bottom of this channel is not clearly visible in Fig. 6c. However, a big difference, in comparison to line B–B′, is the much lower electrical resistivity of the vadose zone in the eastern portion of line A–A′, at least to the progressive distance of 100 m. On the contrary, the western portion of the line is much more resistive, with a maximum between 100 and 150 m along the line. Below the water table (marked by the white dashed line in Fig. 6b), the resistivity is more uniformly similar to the corresponding values in line B–B′ (Fig. 5a). Here, the EC logs also confirm the electrical resistivity image from ERT. The GPR image (Fig. 6c) is also consistent with the ERT results, as attenuation is much larger on the eastern side of the A–A′ line and, in correspondence of the maximum resistivity feature in Fig. 6b

Fig. 4 Oil contamination is apparent from the simple access to the measurement boreholes (**a**) and (**b**). **c** The sample in the plastic bottle left is not filtered, the sample in the tube on the right (which is the same sample but filtered at 0.45 μm), is transparent. The unfiltered sample has a thin floating oil phase and the brown aqueous phase below is an emulsion
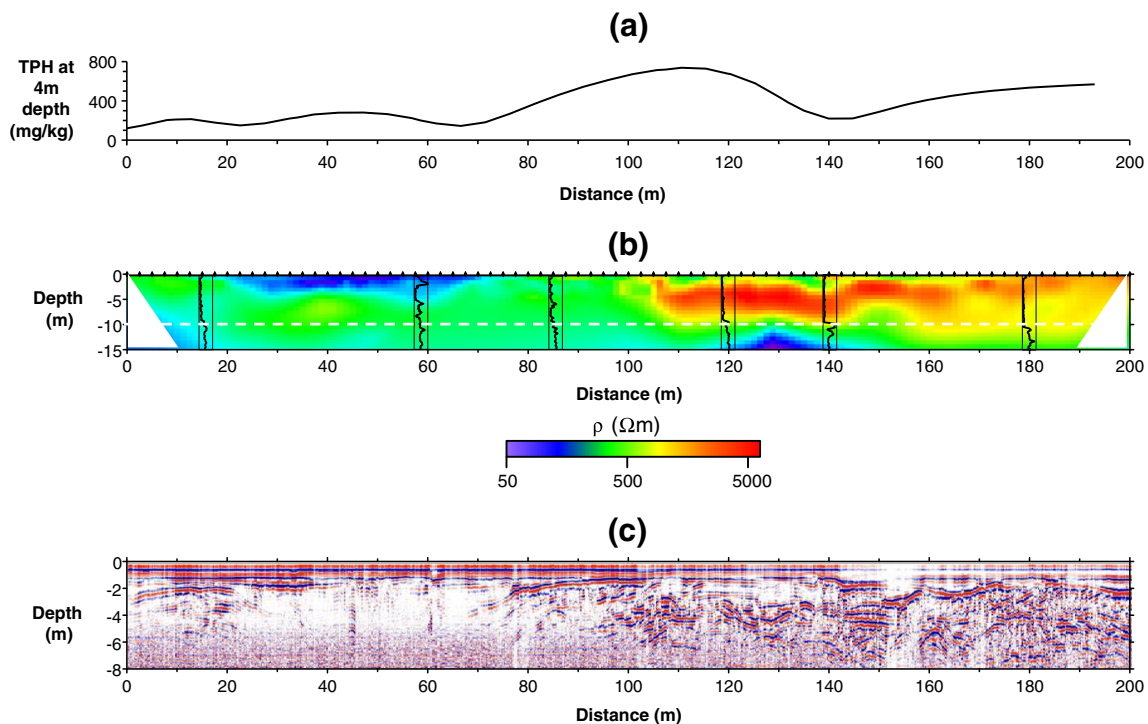
(a)

(b)

Fig. 5 **a** Resistivity image and **b** 100 MHz common offset ground-penetrating radar (GPR) profile along line B–B′ (uncontaminated area, see Fig. 2). Also included in (**a**) are three electrical conductivity (EC) profiles obtained from direct push drilling (the EC scale is linear: 0–15 mS/m).Note the difference in the vertical scale of (**a**) and (**b**). Resistivity data were collected in 9 Feb 2010. GPR data were collected in 9 Mar 2010. EC logs were measured in 8 Mar 2010
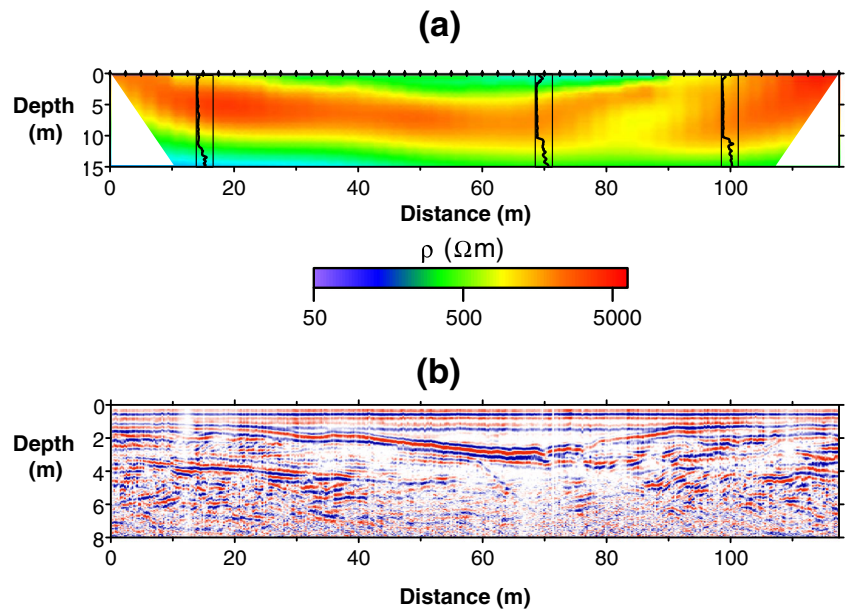
between 100 and 150 m the GPR, produces an intense, detailed scattering.

The comparison between the geophysical data along line A–A′ and the contamination evidence from historical direct push sampling does not clarify a possible link. In Fig. 6a, we show the profile of soil contamination, expressed TPH, interpolated along line A–A′ at 4-m depth. A maximum of TPH is apparent around 110 m (see also the interpolated map in Fig. 2). This maximum does not correspond with the high-resistivity feature to the west or with the low-resistivity feature to the east (Fig. 6b), but seems to span evenly both features. This is not surprising, as the TPH profile is obtained from 3D interpolation of data from some 110 direct push boreholes scattered randomly across the site and drilled from March

(a)

(b)

(c)

Fig. 6 **a** Interpolated soil contamination total petroleum hydrocarbon (*TPH*) profile at 4-m depth; **b** Resistivity image and **b** 100 MHz common offset ground-penetrating radar (GPR) profile along line A–A′ (contaminated area, see Fig. 1). Also included in (**a**) are six electrical conductivity (EC) profiles obtained from direct push drilling (the EC scale is linear: 0–15 mS/m). Note the difference in the vertical scale of (**b**) and (**c**). Resistivity data were collected in 9 Feb 2010. GPR data were collected in 9 Mar 2010. EC logs were measured in 9 Mar 2010

1995 to October 2007 during periodic campaigns spaced about 6 months. From each borehole, five samples were taken at 2-m spacing from 2- to 10-m depth. We expect that this dataset can provide a general picture of the subsurface contamination, but it is clearly very simplified and undersampled in terms of spatial and possibly temporal resolution. Therefore, from this contamination dataset, we cannot expect to find possible correlations between contamination and geophysical response that we know is characterized by a very small scale spatial variability (e.g., Atekwana and Atekwana 2010).

However, the large-scale geophysical data is, in some other way, informative of the possible mechanisms controlling the contamination distribution. Figure 7 shows the soil EC (averaged over the top 6 m of soil) as measured by EMI. Here, some notable features are immediately apparent, namely: (a) a highly conductive linear anomaly in correspondence of the road running north–south across the site, which has been identified with an aqueduct pipeline, and (b) some conductive

features running northwest to southeast that correspond to the conductive palaeo-channels noted in the ERT and GPR sections. The EMI map confirms the continuity of these channels, and a comparison between this map and the subsoil contamination map (Fig. 2) shows that there is a correlation between presence of these channels and the absence of shallow contamination (consider the extent of contamination at 4-m depth in Fig. 2). The contamination in the deeper soil layers is much more homogeneously distributed across the site. This distribution is compatible with the localized infiltration of oil through the most permeable soil zones and the redistribution of hydrocarbon at depth due to the large oscillations of the water table. Consequently, the presence of the palaeo-channels, filled, as discussed earlier, with electrically conductive fine material having low permeability, is likely to have protected the underlying coarser soil from contaminant infiltration from the ground surface.

Even though surface geophysics proves useful in the identification of these large-scale structural features, it is apparent
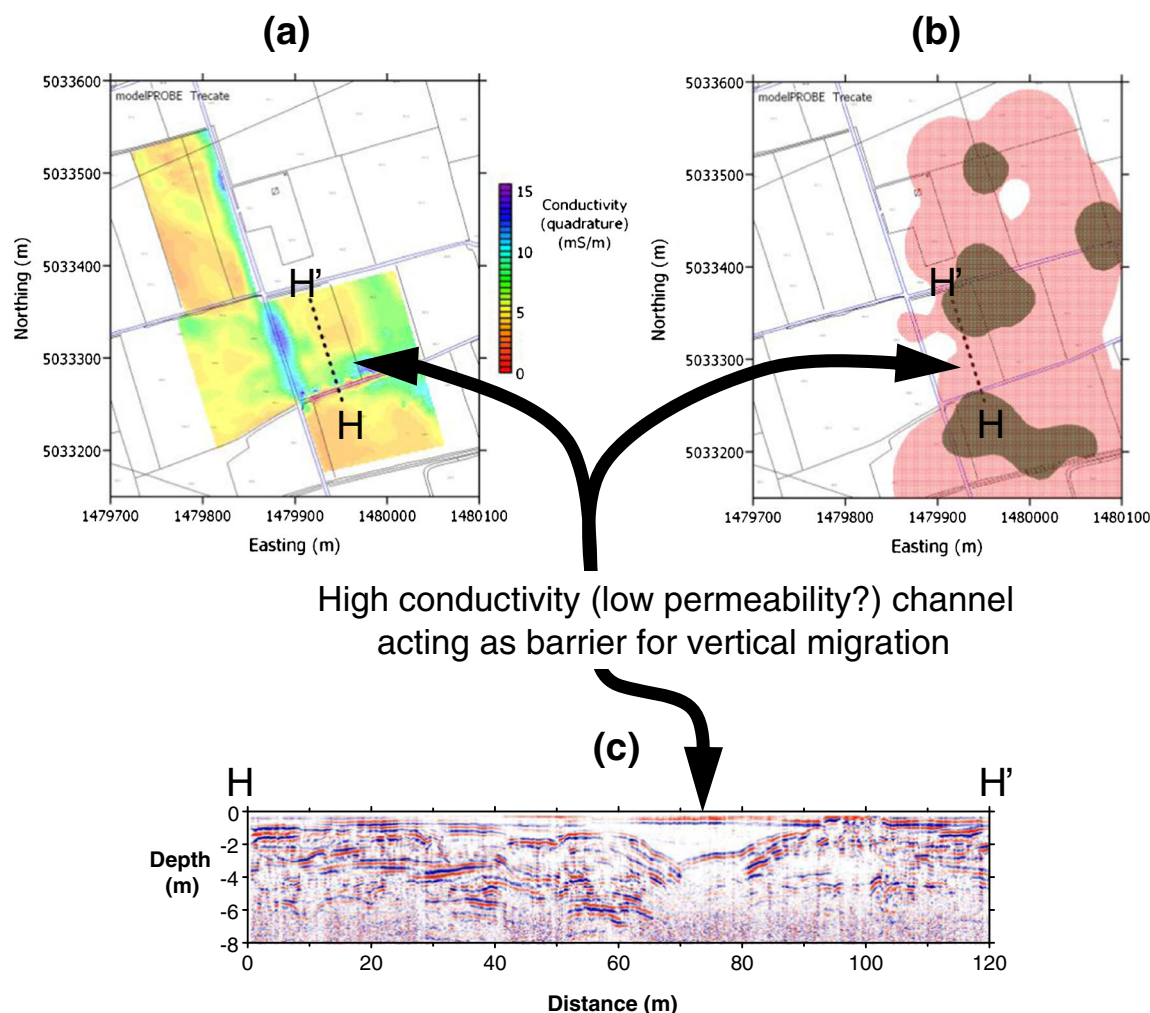
Fig. 7 **a** EM conductivity map obtained using a CMD3 sonde with 5-m penetration. **b** Soil TPH map at 4- and 10-m depths. **c** 100 MHz common offset GPR profile along *line H–H′* shows very clearly the shallow high conductivity channel

how a finer resolution is needed to investigate the correlation between contamination and geophysical signals. This can be achieved through cross-hole measurements.

Cross-hole ERT and GPR

Figure 8 shows the results of cross-hole GPR MOG and ERT acquisitions on the 2009 SoilCAM boreholes in the contaminated area (see Fig. 2 for positioning). The GPR tomographic image (Fig. 8a), here expressed in terms of electromagnetic wave velocity, is readily converted into estimates of volumetric soil moisture content via the Topp et al. (1980) relationship (consider, e.g., Cassiani et al. 2004) and shows clearly the change in soil moisture content in correspondence of the water table, at the time of acquisition (September 2009) at about 6.5 m below ground. A more problematic feature in the GPR image is the presence of a sharp change in GPR velocity at about 12-m depth that does not apparently correspond to a known stratigraphic discontinuity. However, the most troublesome interpretation is linked to the ERT image in Fig. 8b. Here, the only regular feature is given by the shallow low-resistivity palaeo-channel reaching a depth of about 3.5 m and that is already visible from surface geophysics (Fig. 6b). The rest of the inverted resistivity image appears to be very "noisy," with electrical resistivity varying over about one order of magnitude at the very small scale. The most disturbing characteristics of the ERT image is the total lack of correlation with the presence of the water table, measured at about 7.3 m below ground at the time of acquisition (June 2009). The nature of the cross-hole ERT image (and also of the GPR image) in the contaminated zone requires that a more detailed, small-scale analysis be conducted correlating contamination and geophysical signal.

In March 2011, it was possible to conduct cross-hole geophysical measurements also in the new 2011 SoilCAM boreholes. The corresponding results in terms of GPR ZOP are shown in Fig. 9, where a comparison is made with the same type of data collected in the contaminated 2009 SoilCAM boreholes (in both cases, we show the raw radargrams from which it is straightforward to identify the first arrival times that are direct functions of the subsoil moisture content; e.g., Rossi et al. 2012). The difference between the profiles in the uncontaminated (Fig. 9a) and contaminated (Fig. 9b) is apparent. In the uncontaminated zone, the moisture content, and thus the GPR velocity, has a single, sudden drop in correspondence of the water table, while the GPR velocity in the vadose zone is fairly uniform. On the contrary, in the contaminated zone, the velocity profile has a number of variations well above the water table (close to its yearly minimum in March, when the measurements are conducted), and in correspondence of the water table, we observe a much smaller velocity change than in the uncontaminated zone. In addition, a sharp velocity contrast is located about 1 m deeper than the water table, at around 12 m below ground, depth that also corresponds roughly to the absolute yearly minimum observed at the site since the well blowout (1994). This GPR ZOP profile is consistent with the GPR MOG tomographic image shown in Fig. 8a, where the sharp velocity contrast is present at 12 m, and the region between 12 m and the much shallower water table (around 6.5 m below ground in September, i.e., around its yearly maximum) has a GPR velocity intermediate between the value in the unsaturated zone above and the zone deeper than 12 m.

Repeated GPR ZOP measurements were conducted in the borehole pairs in both the contaminated and uncontaminated zones. The results, already converted into estimates of

Fig. 8 Cross-hole ground-penetrating radar (GPR) multiple offset gather and electrical resistivity tomography (ERT) tomographic results collected at the 2009 SoilCAM boreholes (Fig. 2) in the contaminated area
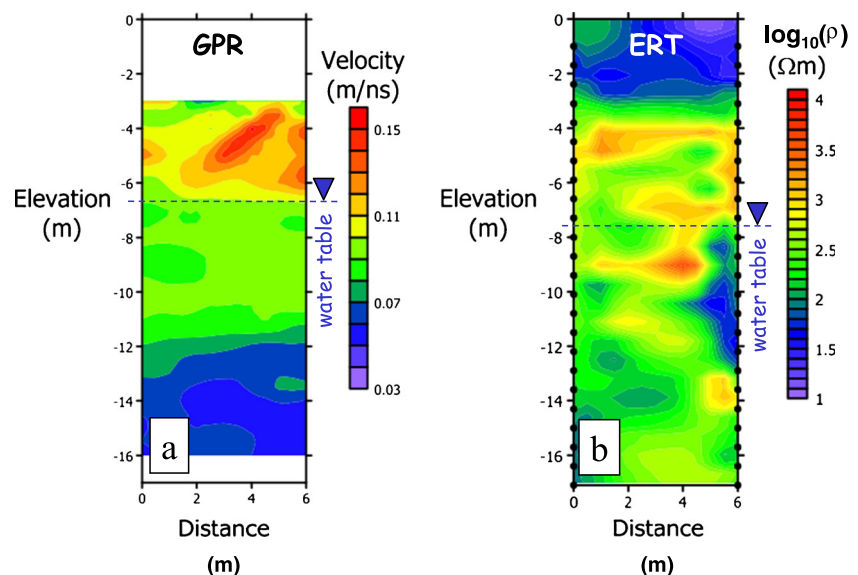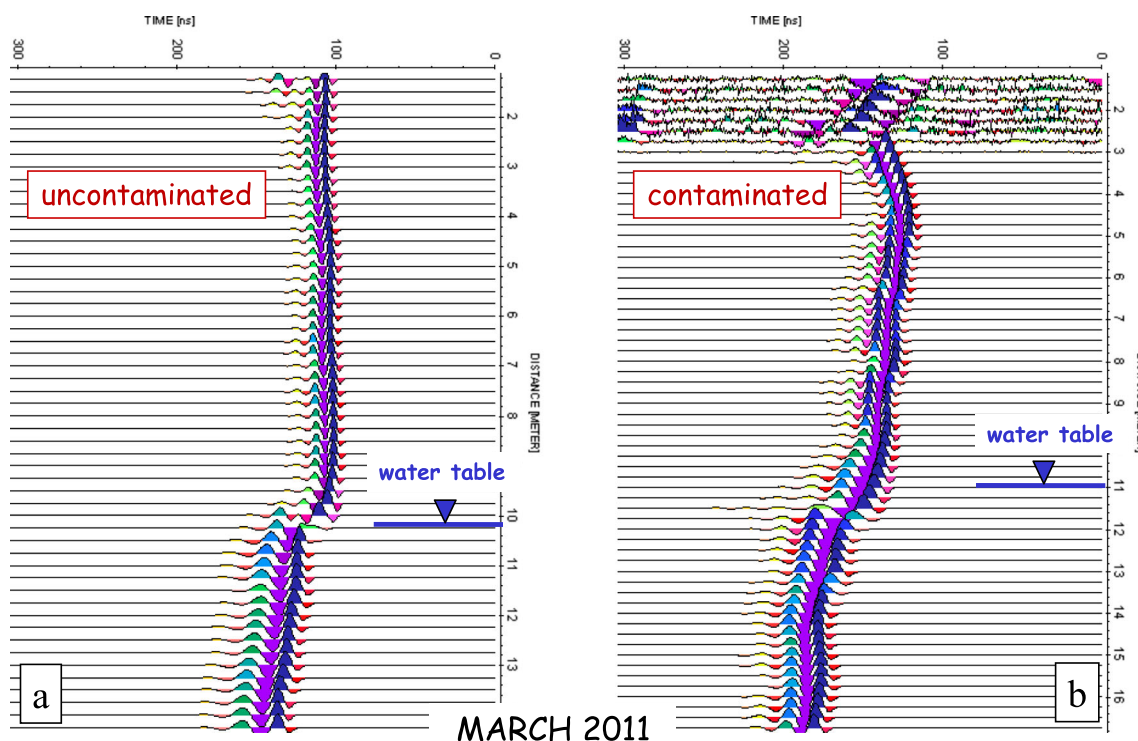
Fig. 9 Cross-hole GPR zero offset profile (ZOP) radargrams collected in March 2011 on **a** the 2011 SoilCAM boreholes in the uncontaminated zone and **b** the 2009 SoilCAM boreholes in the contaminated zone

volumetric soil moisture content via the Topp et al. (1980) relationship, are shown in Fig. 10 and are again very different

for the contaminated versus the uncontaminated zone. In the latter case, the soil moisture varies in the water table
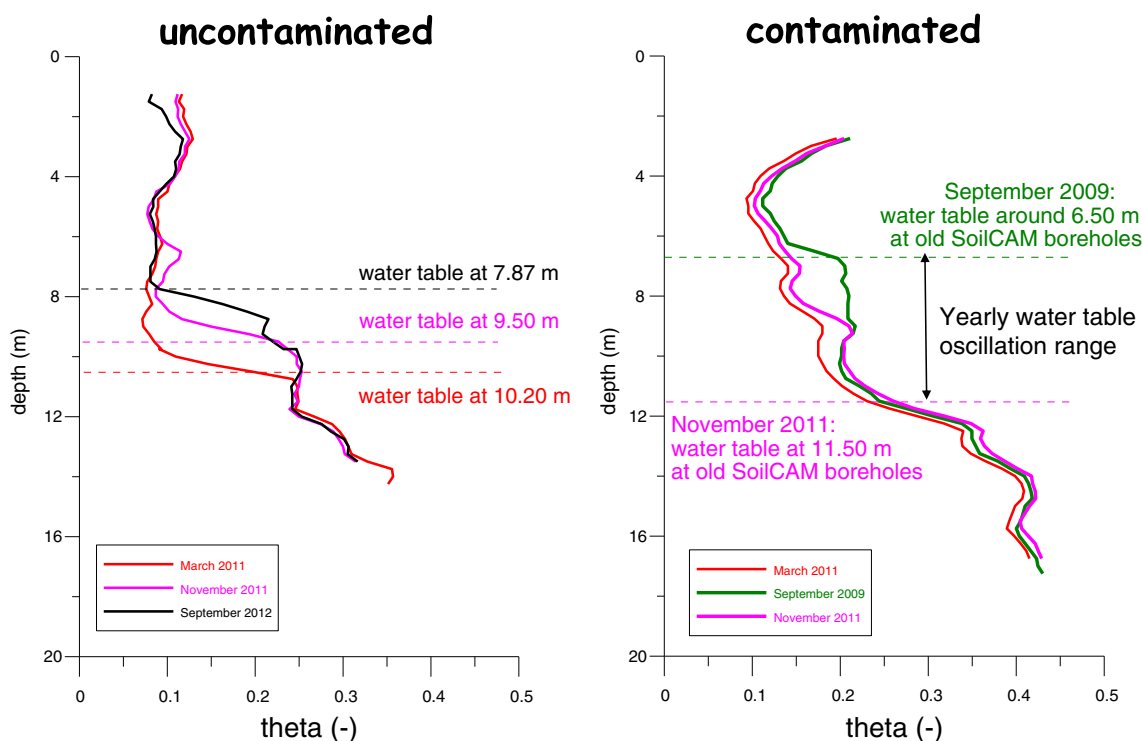

Fig. 10 Estimated soil moisture content profiles derived from cross-hole GPR ZOPs on **a** the 2011 SoilCAM boreholes in the uncontaminated zone and **b** the 2009 SoilCAM boreholes in the contaminated zone at different time instants

Green 1st campaign: 30.08.-04.09.2010: water table ≈ - 6.5 m bgl

Blue 2nd campaign: 11.10-15.10.2010: water table ≈ - 8.5 m bgl

Yellow: 3rd campaign: 10.05.-12.05.2011: water table ≈ - 8.5 m bgl
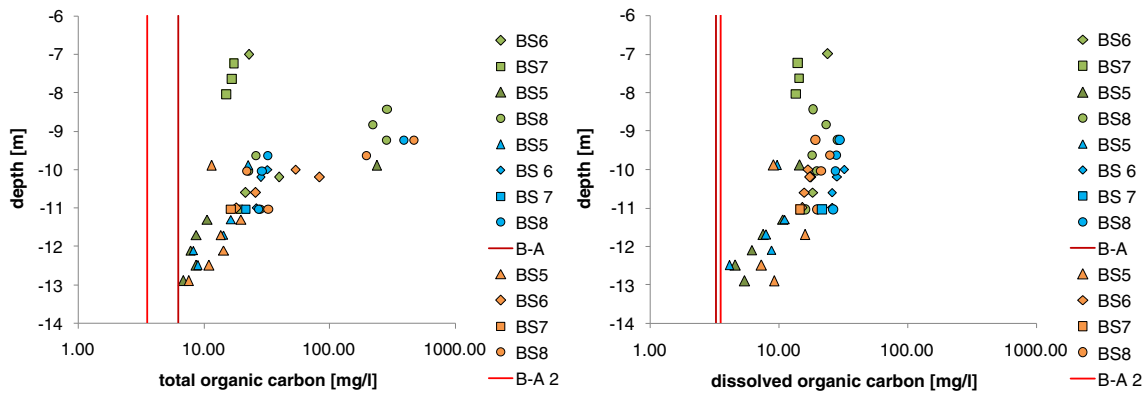
Fig. 11 Total organic carbon and dissolved organic carbon in the three sampling campaigns (*green* 1st, *blue* 2nd, and *yellow* 3rd campaigns) in the four multilevel samplers. The background values are indicated by the *vertical red lines*

oscillation zone from a maximum of about 0.25, compatible with the in situ porosity of the sediments, to a minimum of about 0.08 that is also a reasonable value for residual moisture content after gravity drainage. On the contrary, in the contaminated zone, the range of oscillation of soil moisture content goes from a minimum of 0.14 to a maximum of 0.21, indicating the likely presence of a further phase occupying part of the pore space (at least 4 %, considering the between the highest water moisture content and the minimum porosity of 25 % observed in the uncontaminated sediments). A second effect

may be clogging of pore throats by biomass, which is likely to grow to a large extent in the presence of abundant substrate and reduce permeability (consider, e.g., Brovelli et al. 2009). In addition, it is likely that this oil phase reduces also permeability to water, thus hindering the water drainage when the water table drops and keeping the residual moisture content much higher than in the clean sediments. Note, however, that in both zones, the volumetric soil moisture reaches higher values at depths larger than 12 m, indicating a larger porosity below that depth. This may point towards the fact that around

Fig. 12 Comparison between total organic carbon (*TOC*) measured during the three sampling campaigns in the four multilevel samplers (*left*) and TOC measured in the soil from cores retrieved from two of the multilevel sampler boreholes (*right*)
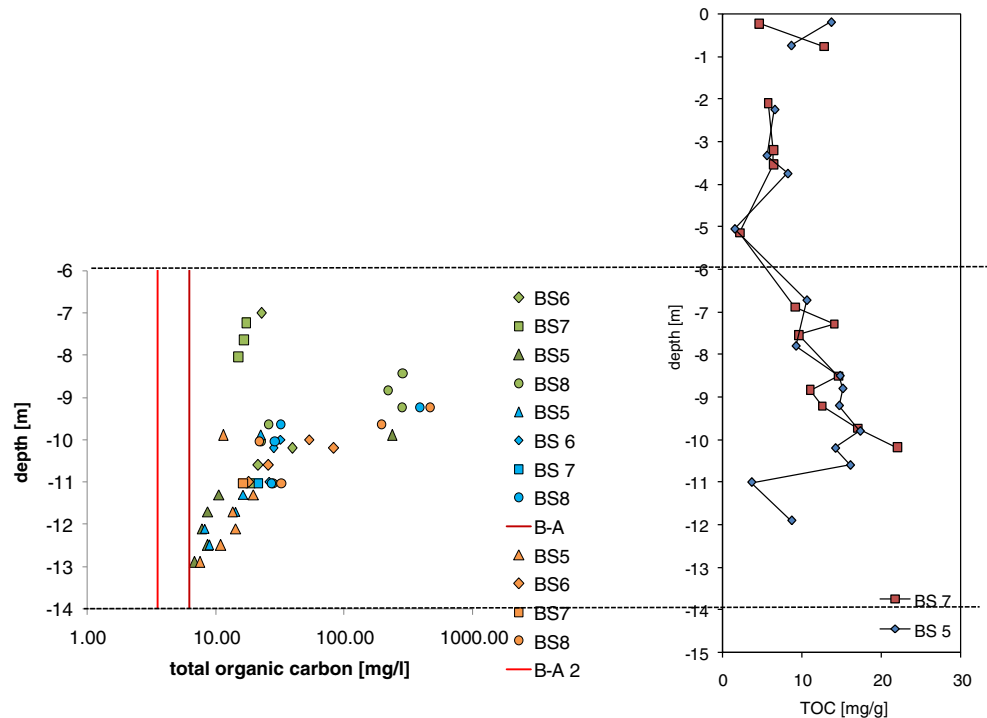
12 m, there is effectively a stratigraphic discontinuity, previously not recognized.

Small-scale contamination data and comparison with geophysical results

Figure 10 shows the TOC and DOC concentrations in the groundwater during three sampling campaigns in the four multilevel samplers BS5 to BS8. Our laboratory analysis showed that, at the Trecate site, the relationship between TOC and TPH in groundwater and soil samples is linear with a slope very close to 1. As TPH was only measured dur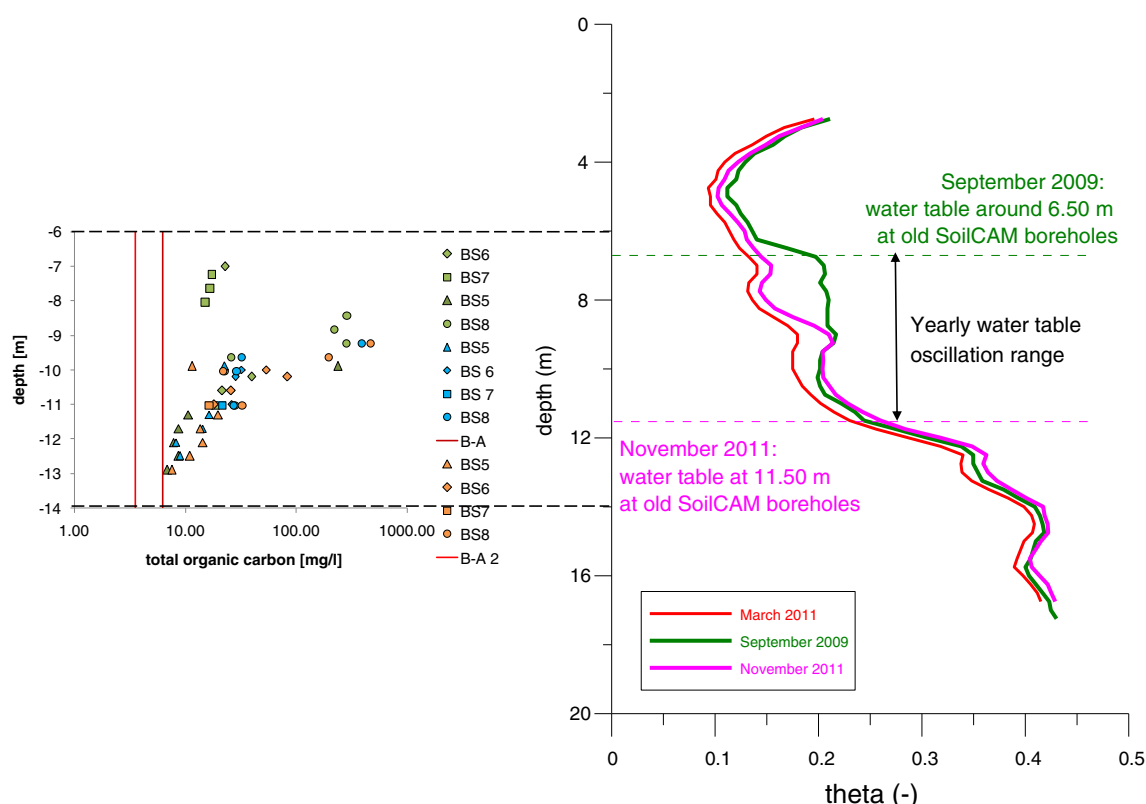ing one sampling campaign, we will therefore use TOC as a proxy for TPH in the following sections. The difference between TOC and DOC consists of organic carbon which does not pass a >0.45-μm filter. This is mainly free-phase oil and oil droplets at this site, which can be concluded from the 1:1 relationship between TOC and TPH and visual inspection. Deviations between TOC and TPH in a naturally carbon poor environment as an aquifer can occur through analytical noise, the presence of microbes and degradation products of hydrocarbons. Figure 11 shows that free-phase oil and oil droplets >0.45 μm are concentrated at depths between 8.5 and 10 m. Note that during campaigns 2 and 3, this depth is just below

the water table, while during campaign 1, the water table is more than 1.5 m higher. Obviously, a large amount of oil remains in place, despite the large water table fluctuations. Note also that this free phase is not completely trapped as residual phase, because in the depths from 8.5 to 10 m free phase and colloidal oil was recovered. Below 10 m, the amount of free and colloidal phase is greatly reduced within a quite sharp boundary, and most of the hydrocarbons are present as dissolved phase (or at least in emulsion with droplets<0.45 μm) with diminishing concentrations towards deeper zones. The depth of 10 m also coincides with the groundwater level beginning of February, which was the month when the oil blowout occurred. It seems that the present situation is still highly influenced by the initial conditions of the spreading oil immediately after the blowout, when oil could freely infiltrate to the top of the water table at about 10-m depth. TOC in the solid phase derived from the soil cores of BS5 and BS7 is shown in Fig. 12 and compared with TOC in water samples: the correspondence between the two profiles is generally very good, but the presence of oily phase seems to cover a wider depth range in the soil core than in the groundwater samples. This may be because groundwater concentrations reflect rather the presence of mobile oil, while from the solid phase concentrations alone, it is not possible
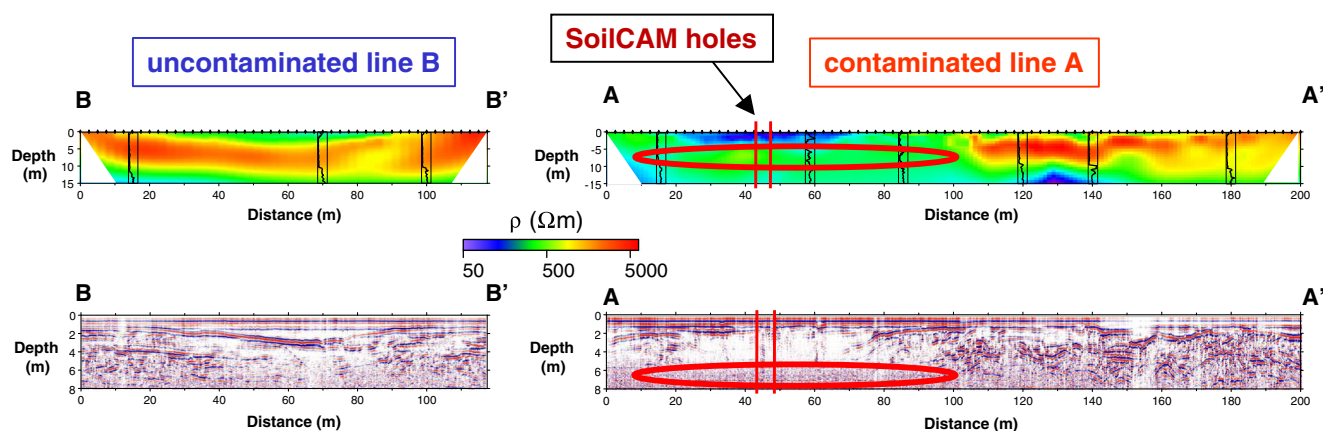

Fig. 13 Comparison between total organic carbon measured during the three sampling campaigns in the four multilevel samplers (*left*) and estimated soil moisture content profiles derived from cross-hole GPR zero offset profiles on the 2009 SoilCAM boreholes in the contaminated zone at different time instants (*right*)

to distinguish trapped and mobile NAPL. It is interesting to note how the zone with trapped and mobile oil phase corresponds clearly with the anomalous zone in the GPR ZOP profiles, as shown in Fig. 13. This comparison corroborates our hypothesis that the anomalously small soil moisture content oscillation range measured by GPR ZOP is indeed caused by the presence of substantial volumes of oil phase.

As discussed above, biodegradation of hydrocarbons results in the production of CO_2, when hydrocarbons are completely mineralized. CO_2 dissolves in water to form carbonic acid, which dissociates into protons and hydrogen carbonate (measured as TIC; Christensen et al. 2000). This lowers the pH and increases the EC of the pore water. Also, other ionic species are produced during oxidation of hydrocarbons by different TEAs. After the depletion of dissolved oxygen and nitrate, manganese and iron oxides are reduced, which results in the production of manganese and iron soluble ions (Stumm and Morgan 1996).

Subsequently, sulfate is reduced to sulfide species, and finally methanogenic conditions may occur. The occurrence of the relevant species at the Trecate site, as detected from the multilevel sampler system, is shown in Fig. 14. Most likely the microbiological activity results in the pronounced changes of the geochemistry in the depths from 8.5 to 11 m. The relationship of the geochemical parameters and microbiological activity at this site is shown by Arato et al. (2013). In this zone, the microbial activity leads to a pronounced change of pore water EC that is increased nearly by a factor of 3 (Fig. 14). Such a strong increase in EC is likely to be observable via ERT. Concomitant to the production of TIC, the redox-sensitive species iron (Fig. 14) and manganese (not shown) show their most pronounced increase between 8.5 and 11-m depth. The trend of dissolved manganese is highly correlated with dissolved Fe (correlation coefficient=0.79; significance level 0.01). Nitrate and nitrite are mostly below detection limit and sulfate concentrations are greatly reduced compared to the background concentration, almost over the entire depth of the water column (not shown). The depletion of sulfate is perfectly consistent with previous evidence (Burbery et al. 2004). The general picture is concurrent with the expected conditions in an oil contaminated aquifer with ferrogenic and sulfidogenic conditions. Sulfate is reduced upstream of the multi-level samplers. The dispersive mixing of the groundwater results in depletion of sulfur species (also nitrate/nitrite) over the entire water column until it

Fig. 14 Concentrations of total inorganic carbon (*TIC*, i.e., hydrogen carbonate), total iron, and electrical conductivity from groundwater extracted from the multilevel samplers during the three field campaigns

Fig. 15 Electrical conductivity (microsiemens per centimeter) in the ports of BS5 to BS8 on the first sampling campaign (August–September 2010). Diameter of the circles corresponds to electrical conductivity in excess of 250 μS/cm. Background values were measured in about 200-m distance in well B-A and B-A2

Fig. 16 anomalous high conductivity zone (circled in *red*) corresponding along the contaminated line A–A′ to the region where hydrocarbon contamination and intense micro-biological activities are likely to exist.

Note the location of the 2009 SoilCAM boreholes along this line (see Fig. 2 for a map)

reaches the multi-level samplers, which is located in the centre of the contaminant area. In contrast, reduced iron and manganese species have a shorter transport distance due to sorption and precipitation reactions at the fringes of the iron/manganese reduction zones (Baedecker et al. 1993; Bennett et al. 1993). Therefore, the reduced iron and manganese species, which are produced upstream of the multi-level samplers are not transported advective dispersively far enough to result in a homogeneously mixed water column with respect to iron and manganese species. This distribution of redox-sensitive species is, to some degree, contradicting the common assumption that zones with species indicating lower redox potentials should be surrounded by zones with species indicating higher redox potentials (Lyngkilde and Christensen 1992). It is apparent from the hydrogeochemical data that there is a strong correlation between the substantial increase of EC and the hydrogeochemical parameters, most likely resulting from the microbiological activity (correlation coefficients of EC with DOC 0.72, Fe 0.82, Mn 0.79, HCO3– 0.57; all on a 0.01 significance level). The spatial distribution of pore-water EC in excess of the background value is shown in Fig. 15: it is quite apparent that this spatial distribution is quite erratic, with very strong differences (around a factor of 3) over a very short distance (note that the multilevel sampler boreholes are aligned at about 1-m distance from each other). As these multilevel sampler boreholes practically cover the region between the 2009 SoilCAM boreholes, it comes as no surprise if such a strong variability in EC is mirrored in the corresponding ERT image to the extent that the variability induced by geochemical processes in the smearing zone is so large as to hide the expected effect of the water table (Fig. 8b). Most important, it is apparent from the biogeochemical data that there is a strong correlation between the presence of hydrocarbon contamination and a substantial increase of EC, most likely caused by microbiological activities.

Conclusions

Our results at the Trecate site confirm that geophysics can have a key role in the definition of structures and contaminant distribution at contaminated sites. The knowledge of structure is likely to have a strong influence on contaminant distribution, as it controlled the oil infiltration at the time of accident. Our geophysical characterization shows structural features that are likely to have controlled such infiltration process. But more interesting is the analysis of the correlation between geophysical signals and contamination. This analysis was made possible by the joint availability of small-scale cross-hole geophysical data (both ERT and GPR) and small-scale geochemical data (from multilevel samplers). Note that geochemical processes and geophysical measurements do not necessarily have the same spatial scale, but we tried to achieve a spatial resolution of the geophysical measurements fine enough to detect the spatial variability observed in the geochemical data that appears to be in the meter scale. The results from multilevel samplers suggest that a strong geochemical signal, possibly coming from microbiological activity, is taking place around the smearing zone, between 6- and 11-m depth, where a large presence of free and trapped hydrocarbon phase is detected. This presence is confirmed by the reduced variability of soil moisture content in this zone, as well identified by cross-hole GPR measurements. In this zone, we observe a depletion of oxygen, nitrate, and sulfate and an increase of iron and manganese in solution, with a corresponding increase also of TIC. These signatures are compatible with microbiological activity linked to petroleum biodegradation. The main overall effect is a net increase, as large as a factor of three, of pore-water EC, showing a marked spatial variability. This signal is perfectly detectable by cross-hole ERT, also showing the same spatial variability.

This is a fundamental piece of information that allows us to revisit the surface ERT data (Fig. 16): the presence of a low

electrical resistivity region along line A–A′, above the water table and generally around it oscillations, corresponds to the region where the geochemical signals are detected and is likely to be correlated with biological activity triggered by contamination. In this manner, we can use geophysical data to extrapolate the detailed, but localized, geochemical information and potentially draw general conclusions about the larger-scale spatial distribution of hydrocarbon contamination at the Trecate site.

References

Abdel Aal GZ, Slater LD, Atekwana EA (2006) Induced-polarization measurements on unconsolidated sediments from a site of active hydrocarbon biodegradation. Geophysics 71:H13–H24

Annan AP (2005) GPR methods for hydrogeological studies. In: Rubin Y, Hubbard SS (eds) Hydrogeophysics, Ser. 50. Springer, Dordrecht, pp 185–214

Arato A, Wehrer M, Biró B, Godio A (2013) Integration of geophysical, geochemical and microbiological data for a comprehensive small-scale characterization of an aged LNAPL-contaminated site. Environ Sci Pollut Res. doi:10.1007/s11356-013-2171-2, this issue

Atekwana EA, Atekwana EA (2010) Geophysical signatures of microbial activity at hydrocarbon contaminated sites: a review. Surv Geophys 31:247–283. doi:10.1007/s10712-009-9089-8

Atekwana EA, Sauck WA, Werkema DD (2000) Investigations of geoelectrical signatures at a hydrocarbon contaminated site. J ApplGeophys 44(2–3):167–180. doi:10.1016/S0926-9851(98)00033-0

Atekwana EA, Sauck WA, Abdel Aal GZ, Werkema DD (2002) Geophysical investigation of vadose zone conductivity anomalies at a hydrocarbon contaminated site: implications for the assessment of intrinsic bioremediation. J Environ Eng Geophys 7:103–110

Atekwana EA, Atekwana EA, Werkema DD, Duris JW, Rossbach S, Sauck WA, Cassidy DP, Means J, Legall FD (2004a) In situ apparent conductivity measurements and microbial population distribution at a hydrocarbon-contaminated site. Geophysics 69(1):56–63. doi:10.1190/1.1649375

Atekwana EA, Atekwana EA, Rowe RS, Werkema DD, Legall FD (2004b) The relationship of total dissolved solids measurements to bulk electrical conductivity in an aquifer contaminated with hydrocarbon. J Appl Geophys 56:281–294

Atekwana EA, Atekwana E, Legall FD, Krishnamurthy RV (2004c) Field evidence for geophysical detection of subsurface zones of enhanced microbial activity. Geophys Res Lett 31, L23603

Atekwana EA, Atekwana EA, Legall FD, Krishnamurthy RV (2005) Biodegradation and mineral weathering controls on bulk electrical conductivity in a shallow hydrocarbon contaminated aquifer. J Contam Hydrol 80:149–167

Baedecker MJ, Cozzarelli IM, Eganhouse RP, Siegel DI, Bennett PC (1993) Crude-oil in a shallow sand gravel aquifer 3. Biogeochemical reactions and mass-balance modeling in anoxic groundwater. Appl Geochem 8(6):569–586. doi:10.1016/0883-2927(93)90014-8

Bekins BA, Cozzarelli IM, Godsy EM, Warren E, Essaid HI, Tuccillo ME (2001) Progression of natural attenuation processes at a crude oil spill site: II. Controls on a spatial distribution of microbial populations. J Contam Hydrol 53(3–4):387–406. doi:10.1016/S0169-7722(01)00175-9

Bennett PC, Siegel DE, Baedecker MJ, Hult MF (1993) Crude oil in a shallow sand and gravel aquifer: 1. Hydrogeology and inorganic geochemistry. Appl Geochem 8(6):529–549. doi:10.1016/0883-2927(93)90012-6

Benson AK, Payne KL, Stubben MA (1997) Mapping groundwater contamination using dc resistivity and VLF geophysical methods—a case study. Geophysics 62:80–86

Bermejo JL, Sauck WA, Atekwana EA (1997) Geophysical discovery of a new LNAPL plume at the former Wurtsmith AFB, Oscoda, Michigan. Ground Water Monit Remediat 17:131–137

Binley AM, Kemna A (2005) DC resistivity and induced polarization methods. In: Rubin Y, Hubbard SS (eds) Hydrogeophysics. Water Sci. Technol. Library, Ser. 50. Springer, New York, pp 129–156

Binley, A., Ramirez, A., Daily, W. (1995) Regularised image reconstruction of noisy electrical resistance tomography data. In: Beck MS, Hoyle BS, Morris MA, Waterfall RC, Williams RA (eds), Process tomography — 1995. Proceedings of the 4th Workshop of the European Concerted Action on Process Tomography, Bergen, 6–8 April 1995, pp. 401– 410.

Binley AM, Cassiani G, Deiana R (2011) Hydrogeophysics—opportunities and challenges. B GEOFIS TEOR APPL 51(4):267–284

Bradford JH (2007) Frequency-dependent attenuation analysis of ground-penetrating radar data. Geophysics 72:J7–J16. doi:10.1190/1.2710183

Brandt CA, Becker JM, Porta A (2002) Distribution of polycyclic aromatic hydrocarbons in soils and terrestrial biota after a spill of crude oil in Trecate, Italy. Environ Toxicol Chem 21:1638–1643

Brovelli A, Malaguerra F, Barry DA (2009) Bioclogging in porous media: model development and sensitivity to initial conditions. Environ Model Softw 24:611–626

Burbery L, Cassiani G, Andreotti G, Ricchiuto T, Semple KT (2004) Well test and stable isotope analysis for the determination of sulphate-reducing activity in a fast aquifer contaminated by hydrocarbons. Environ Pollut 129(2):321–330

Cassiani G, Strobbia C, Gallotti L (2004) Vertical radar profiles for the characterization of deep vadose zones. Vadose Zone J 3:1093–1115

Cassiani G, Bruno V, Villa A, Fusi N, Binley AM (2006) A saline tracer test monitored via time-lapse surface electrical resistivity tomography. J Appl Geophys 59:244–259. doi:10.1016/j.jappgeo2005.10.007

Cassidy NJ (2007) Evaluating LNAPL contamination using GPR signal attenuation analysis and dielectric property measurements: practical implications for hydrological studies. J Contam Hydrol 94:49–75

Che-Alota V, Atekwana EA, Atekwana EA, Sauck WA, Werkema DD (2009) Temporal geophysical signatures due to contaminant mass reduction. Geophysics 74(4):B113–B123. doi:10.1190/1.3139769

Chen J, Hubbard SS, Williams KH, Flores Orozco A, Kemna A (2012) Estimating the spatiotemporal distribution of geochemical parameters associated with biostimulation using spectral induced polarization data and hierarchical Bayesian models. Water Resour Res 48, W05555. doi:10.1029/2011WR010992

Christensen TH, Bierg PL, Banwart SA, Jakobsen R, Heron G, Albrechtsen HJ (2000) Characterization of redox conditions in groundwater contaminant plumes. J Contam Hydrol 45(3–4):165–241

Christensen O, Cassiani G, Diggle PJ, Ribeiro P, Andreotti G (2004) Statistical estimation of the relative efficiency of natural attenuation mechanisms in contaminated aquifers. Stoch Env Res Risk A 18:339–350

Daily W, Ramirez A, LaBrecque D, Nitao J (1992) Electrical resistivity tomography of vadose water movement. Water Resour Res 28(5):1429–1442

Daily W, Ramirez A, LaBrecque D, Barber W (1995) Electrical-resistance tomography at the Oregon-Graduate-Institute. J Appl Geophys 33(4):227–237. doi:10.1016/0926-9851(95)00004-L

Deiana R, Cassiani G, Villa A, Bagliani A, Bruno V (2008) Model calibration of a water injection test in the vadose zone of the Po River plain using GPR cross-hole data. Vadose Zone J 7:215–226. doi:10.2136/vzj2006.0137

Everett M, Meju M (2005) Near-surface controlled-source electromagnetic induction. In: Rubin Y, Hubbard SS (eds) Hydrogeophysics. Water Sci. Technol. Library, Ser. 50. Springer, New York, pp 157–183

Flores Orozco A, Williams KH, Long PE, Hubbard SS, Kemna A (2011) Using complex resistivity imaging to infer biogeochemical processes associated with bioremediation of a uranium-contaminated aquifer. J Geophys Res 116, G03001

Flores Orozco A, Oberdorster C, Zschornack L, Leven C, Dietrich P, Weiss H (2012) Delineation of subsurface hydrocarbon contamination at a former hydrogenation plant using spectral induced polarization imaging. J Contam Hydrol 136:131–144. doi:10.1016/j.jconhyd.2012.06.001

French HK, van der Zee SEATM, Meju M (2009) SoilCAM: soil contamination: advanced integrated characterisation and time-lapse monitoring. Rev Environ Sci Biotechnol 8:125–130. doi:10.1007/s11157-009-9158-y

Gasperikova E, Hubbard SS, Watson DB, Baker GS, Peterson JE, Kowalsky MB, Smith M, Brooks S (2012) Long-term electrical resistivity monitoring of recharge-induced contaminant plume behavior. J Contam Hydrol 142:33–49. doi:10.1016/j.jconhyd.2012.09.007

Kästner M, Cassiani G (2009) ModelPROBE: model driven soil probing, site assessment and evaluation. Rev Environ Sci Biotechnol 8:131–136. doi:10.1007/s11157-009-9157-z

Kemna A, Vanderborght J, Kulessa B, Vereecken H (2002) Imaging and characterisation of subsurface solute transport using electrical resistivity tomography (ERT) and equivalent transport models. J Hydrol 267:125–146

LaBrecque DJ, Ramirez AL, Daily WD, Binley AM, Schima SA (1996) ERT monitoring of environmental remediation processes. Meas Sci Technol 7(3):375–383

Lee JY, Cheon JY, Lee KK, Lee SY, Lee MH (2001) Factors affecting the distribution of hydrocarbon contaminants and hydrogeochemical parameters in a shallow sand aquifer. J Contam Hydrol 50:139–158

Lopes de Castro D, Branco RMGC (2003) 4-D ground penetrating radar monitoring of a hydrocarbon leakage site in Fortaleza (Brazil) during its remediation process: a case history. J Appl Geophys 54:127–144

Lyngkilde J, Christensen TH (1992) Redox zones of a landfill leachate pollution plume (Vejen, Denmark). J Contam Hydrol 10(4):273–289

Mage R, Porta A (2001) Long-term biodegradation of underground and aquifer contamination at Trecate. In: Leeson A, Johnson PC, Hinchee RE, Semprini L, Magar VS (eds) In situ aeration and aerobic remediation book series: bioremediation series, vol 6, issue 10. 6th International In Situ and On-Site Bioremediation Symposium, San Diego, CA, 2001 June 4–7, pp 109–114.

Monego M, Cassiani G, Deiana R, Putti M, Passadore G, Altissimo L (2010) Tracer test in a shallow heterogeneous aquifer monitored via time-lapse surface ERT. Geophysics 75(4):WA61–WA73. doi:10.1190/1.3474601

Osella A, de la Vega M, Lascano E (2002) Characterization of a contaminant plume due to a hydrocarbon spill using geoelectrical methods. J Environ Eng Geophys 7:78–87

Perri MT, Cassiani G, Gervasio I, Deiana R, Binley AM (2012) A saline tracer test monitored via both surface and cross-borehole electrical resistivity tomography: comparison of time-lapse results. J Appl Geophys 79:6–16. doi:10.1016/j.jappgeo.2011.12.011

Petts J. Cairney T, Smith M (1997) Risk-based contaminated land investigation and assessment. Wiley, ISBN: 978-0-471-96608-1, 352 pp

Pumphrey KM, Chrysikopoulos CV (2004) Non-aqueous phase liquid drop formation within a water saturated fracture. Colloids Surf A Physicochem Eng Asp 240(1–3):199–209

Revil A, Titov K, Doussan C, Lapenna V (2006) Applications of the self-potential method to hydrological problems. In: Vereecken H, Binley A, Cassiani G, Kharkhordin I, Revil A, Titov K (eds) Applied hydrogeophysics. Springer-Verlag, Berlin, pp 255–292

Rossi M, Cassiani G, Binley AM (2012) A stochastic analysis of cross-hole GPR zero-offset profiles for subsurface characterization. Vadose Zone J 11(4):CP9–+. doi:10.2136/vzj2011.0078

Sauck WA, Atekwana EA, Nash MS (1998) High conductivities associated with an LNAPL plume imaged by integrated geophysical techniques. J Environ Eng Geophys 2:203–212

Schütze C, Vienken T, Werban U, Dietrich P, Finizola A, Leven C (2012) Joint application of geophysical methods and direct push soil gas surveys for the improved delineation of buried fault zones. J Appl Geophys 82(2012):129–136. doi:10.1016/j.jappgeo.2012.03.002

Sogade JA, Scira-Scappuzzo F, Vichabian Y, Shi WQ, Rodi W, Lesmes DP, Morgan FD (2006) Induced-polarization detection and mapping of contaminant plumes. Geophysics 71(3):B75–B84. doi:10.1190/1.2196873

Stumm W, Morgan JJ (1996) Aquatic chemistry, 3rd edn. Wiley, New York

Tezkan B, Georgescu P, Fauzi U (2005) A radiomagnetotelluric survey on an oil-contaminated area near the Brazi Refinery, Romania. Geophys Prospect 53:311–323

Topp GC, Davis JL, Annan AP (1980) Electromagnetic determination of soil water content: measurements in coaxial transmission lines. Water Resour Res 16:574–582

Werkema DD, Atekwana EA, Endres AL, Sauck WA, Cassidy DP (2003) Investigating the geoelectrical response of hydrocarbon contamination undergoing biodegradation. Geophys Res Lett 30:1647. doi:10.1029/2003GL017346

Willumsen PA, Karlson U (1997) Screening of bacteria, isolated from PAH-contaminated soils, for production of biosurfactants and bioemulsifiers. Biodegradation 7(5):415–423